Extended critical phase in quasiperiodic quantum Hall systems

Jonas F. Karcher [1], Romain Vasseur [2] and Sarang Gopalakrishnan [3]
[1] Department of Physics, Pennsylvania State University, University Park, Pennsylvania 16802, USA
[2] Department of Physics, University of Massachusetts, Amherst, Massachusetts 01003, USA
[3] Department of Electrical and Computer Engineering, Princeton University, Princeton, New Jersey 08544, USA

(Received 15 November 2023; revised 18 January 2024; accepted 7 February 2024; published 26 February 2024)

We consider the effects of quasiperiodic spatial modulation on the quantum Hall plateau transition by analyzing the Chalker-Coddington network model with quasiperiodically modulated link phases. In the conventional case (uncorrelated random phases), there is a critical point separating topologically distinct integer quantum Hall insulators. Surprisingly, the quasiperiodic version of the model supports an extended critical phase for some angles of modulation. We characterize this critical phase and the transitions between critical and insulating phases. For quasiperiodic potentials with two incommensurate wavelengths, the transitions we find are in a different universality class from the random transition. With the addition of more wavelengths they undergo a crossover to the uncorrelated random case. We expect our results to be relevant to the quantum Hall phases of twisted bilayer graphene or other moiré systems with large unit cells.

DOI: 10.1103/PhysRevB.109.064208

I. INTRODUCTION

The integer quantum Hall (IQH) effect is the remarkably robust quantized Hall response of two-dimensional electron gases subject to a strong external magnetic field. Disorder plays a crucial part in stabilizing plateaus of density with the quantized Hall response [1]: almost all the single-particle states in the IQH regime are Anderson localized, and moving the Fermi energy in a region of localized states does not change the response. Plateau transitions occur when the Fermi level crosses an extended state, leading to a jump in the quantized response. In the "standard" IQH scenario, with uncorrelated randomness, the plateau transition is a critical point, about which many open questions remain [2–7]. However, in many present-day realizations of IQH physics, such as graphene grown on a substrate and twisted bilayer materials in a magnetic field, the dominant spatial modulations are not uncorrelated, but quasiperiodic (QP). The study of electronic states—and, more generally, wave propagation—in quasiperiodic media has been a topic of intense experimental interest [8–12]. Wave functions in quasiperiodic media also undergo Anderson localization, but the nature of the localization transition is different from that in random systems. The best-studied example of a quasiperiodic potential is the Aubry-André model in one dimension [13], which exhibits a transition from ballistic to localized states as the potential strength is tuned. (In contrast, random systems in one dimension are always in the localized phase [14].) Recently, the localization transition in higher-dimensional or longer-range quasiperiodic systems was also studied [10,15–22], but not for the symmetry class [23] corresponding to the plateau transition. In addition to the ballistic and localized phases, some of these models have been shown to exhibit unusual intermediate phases, but they have not yet been classified.

In this work we study the effects of quasiperiodic spatial modulations on the IQH plateau transition. Following the standard approach to the disordered case, we study Chalker-Coddington (CC) network models [24,25] with quasiperiodically modulated link phases. In most of the paper, we consider the simplest type of quasiperiodic modulation, namely, the case in which the parameters in the network model are modulated with a single wavelength that is incommensurate with the underlying lattice structure. This case is also the most relevant to potential near-term experiments, e.g., on moiré materials in magnetic fields [9], graphene grown on a substrate, and ultracold atomic gases in synthetic magnetic fields [26]. However, in order to understand how the quasiperiodic transition and the random one are related, we also consider systems with multiple incommensurate wavelengths. Our main results come from direct numerical calculations of the single-particle states, but our conclusions are also qualitatively supported by a real-space renormalization group treatment of a simplified model.

Outline of this work

In Sec. II A, we introduce the Chalker-Coddington network that we focus on and the scaling theory we use to probe its phase diagram (Sec. II C). Our main results are as follows. We show that the plateau transition in the quasiperiodic network model with two incommensurate wave vectors ("tones") lies in a different universality class from the standard plateau transition in Sec. III. Indeed, the phase diagram of the network model is richer in the two-tone quasiperiodic case: instead of two insulating phases separated by a critical point, we find (in some parameter ranges, see Sec. III A) a critical *phase* between the two insulating phases. When this critical phase is present, the quantized Hall plateaus are separated by a metallic phase in which the Hall conductivity is not quantized. In addition, even for parameters that show a direct transition between two insulating phases, the critical exponents at this transition differ from the exponents in the standard plateau transition (see Sec. III B). Adding more tones induces

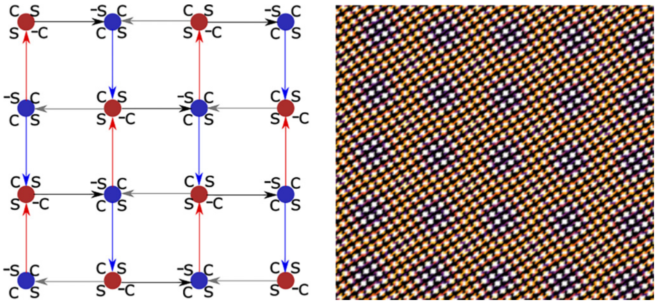

FIG. 1. Network model. Left: Visualization of the scattering matrix $\mathcal{S}$ of the Chalker-Coddington network model defined on a square lattice. The degrees of freedom live on the links, receive phases while propagating, and can scatter into each other at the nodes weighted by $\pm s \equiv \pm\sin(\rho)$ or $\pm c \equiv \pm\cos(\rho)$. At $\rho = \pi/4$, the quantum Hall transition occurs. Right: Quasiperiodic configuration ($\theta = \pi/6.2$) for the link phases. The scattering angles are tuned to criticality $\rho = \pi/4$ for the ED numerics.

a crossover to the random critical behavior, but not when the additional tones are sufficiently weak, which is discussed in Sec. IV.

II. MODELS AND METHODS

Here we introduce the Chalker-Coddington network that we focus on (Sec. II A) and the Ando model (Sec. II B) that we consider for the crossover to randomness. In Sec. II C, we introduce the scaling theory necessary to find the phase diagrams of our models.

A. Quasiperiodic Chalker-Coddington network

The CC network model [24] is an effective model of electronic states near a plateau transition. It is a model of chiral degrees of freedom defined on the links of a square lattice, which scatter either left or right at the vertices of the lattice (Fig. 1). Each vertex hosts a unitary scattering matrix $\mathcal{S}$, with scattering weights $\pm s \equiv \pm\sin(\rho)$ or $\pm c \equiv \pm\cos(\rho)$. The network model can be interpreted as a Floquet unitary evolution [27]. Its single-particle spectrum lies in the unit circle of the complex plane, and the eigenvalues $e^{i\omega}$ can be labeled by the real quasienergy ω. Deep in the two localized phases, $|c| \approx 1$ and $|s| \approx 1$, the eigenstates of the network model are localized on single plaquettes and rotate clockwise (counterclockwise) for $|c| \approx 1$ ($|s| \approx 1$). For random potentials, the plateau transition occurs at the self-dual point $\rho_s = \pi/4$. Knowing the location of the self-dual point allows us to eliminate a class of finite size effects related to the uncertainty of the position of the critical point. We denote the distance to this point by $d = \rho - \rho_s$. In the quasiperiodically modulated model there still is symmetry around the self-dual point; in other words, ρ can be exchanged for $\rho_s - \rho$ (and $\rho \rightarrow \pi + \rho$).

We choose link phases $\phi(r)$ at each link r defined over the quasiperiodic function (following Refs. [15,21]):

$$\phi(r) = 2\pi \sum_{i=1,2} \cos\left(\sum_j A_{ij} r_j + \gamma_i\right),$$
$$A_{11} = A_{22} = \varphi\cos\theta, A_{12} = -A_{21} = \varphi\sin\theta, \qquad (1)$$

where $\varphi = (1-\sqrt{5})/2$ is the golden ratio and $\gamma_{1,2}$ are phases. We show an example configuration ($\theta = \pi/6.2$) for the link phases; it exhibits a superlattice moiré pattern with an emergent length scale of several lattice constants. At $\pi/5$, the twist $\cos(\pi/5)$ becomes proportional to the golden ratio, and this makes the phases commensurate with the lattice in one direction. Further, at π/θ with large θ, there is basically no rotation $[\cos(\pi/\theta) \approx 1]$. These end points determine the range of θ investigated in this work. In order to avoid the need for rational approximants of the angles θ and the golden ratio matching the system size (see discussions in Refs. [15,21]), we choose open boundary conditions. This comes at the expense of having to omit values of the wave function close to the boundary in the multifractal analysis.

B. Quasiperiodic Ando model

We further consider the Ando model in the symplectic class:

$$H = \sum_{r,\sigma} \epsilon_r c^\dagger_{r,\sigma} c_{r,\sigma} + \sum_{\sigma\sigma'} [c^\dagger_{r,\sigma} T^{\hat{x}}_{\sigma\sigma'} c_{r+\hat{x},\sigma'} + c^\dagger_{r,\sigma} T^{\hat{y}}_{\sigma\sigma'} c_{r+\hat{y},\sigma'} + \text{H.c.}],$$
$$T^{\hat{x}} = \begin{pmatrix} \frac{\sqrt{3}}{2} & \frac{i}{2} \\ \frac{i}{2} & \frac{\sqrt{3}}{2} \end{pmatrix}, \qquad T^{\hat{y}} = \begin{pmatrix} \frac{\sqrt{3}}{2} & \frac{1}{2} \\ -\frac{1}{2} & \frac{\sqrt{3}}{2} \end{pmatrix}. \qquad (2)$$

Quasirandomness enters through the potential ϵ_r. The phase diagram of this model was explored in Ref. [15]. We back up our claims on crossing over to the random fixed point with this model in Sec. IV B.

With this in mind, we define $\epsilon_r = V[w\phi_1(r) + (1-w)\phi_2(r)]$ with two functions $\phi_k(r)$ defined analogous to Eq. (1). The parameter $w \in [0, 1]$ controls the relative strength of the different tones. For the uncorrelated random case to compare to, we choose $\epsilon_r \in [-V/2, V/2]$ independently and uniformly.

C. Scaling theory and observables

At Anderson transitions, there is an infinite continuum of critical exponents, the multifractal spectrum. When the potential is spatially uncorrelated, the multifractal spectrum can be extracted from the scaling of the qth local density of states moments

$$\langle \rho(\omega, r)^q \rangle_\beta \sim \langle \rho(\omega)^q \rangle_\beta \langle |\psi(r)|^{2q} \rangle_\beta \sim L^{-2q-x_q} \qquad (3)$$

in systems where the density of states $\rho(\omega)$ does not scale with the system size. This defines a scaling dimension x_q for each q, the multifractal spectrum.

For correlated potentials, it is necessary to average the wave functions over boxes larger than the correlation volume first before analyzing the moments:

$$\mu_i = \int_{B_i} d^2r\, |\psi(r)|^2, \quad \langle \ln \mu_i \rangle_\beta = \alpha \ln\left(\frac{b}{L}\right). \qquad (4)$$

When one chooses the box size b to scale like the system size, say, $b = L/12$, then the logarithmic average

$$\alpha = \frac{1}{N_B} \sum_i \langle \ln(\mu_i) \rangle_\beta \qquad (5)$$

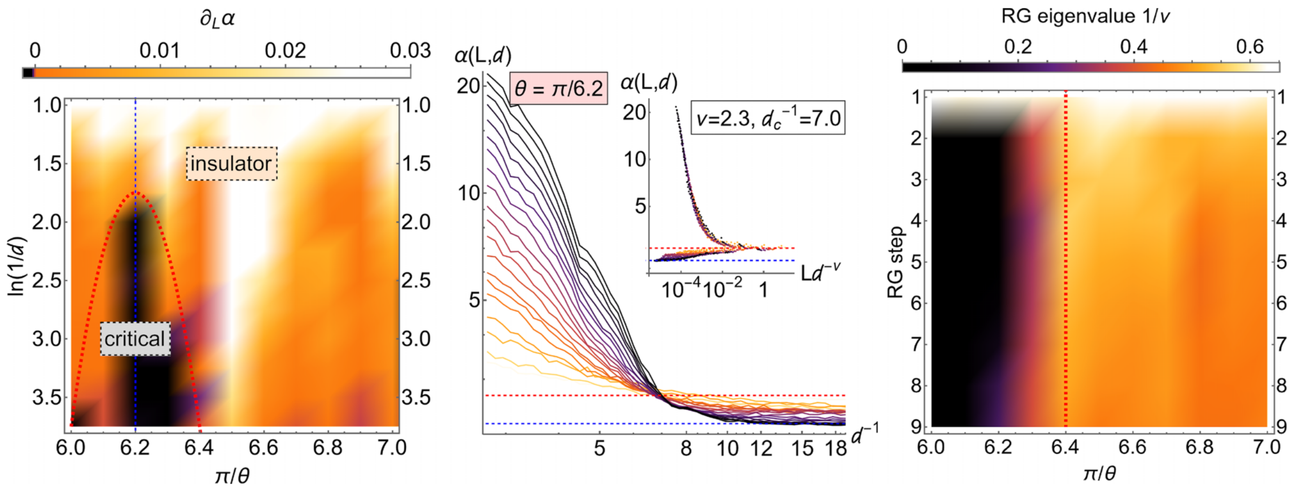

FIG. 2. Phase diagram and stability of the extended critical phase. Left: Derivative $\partial_L \alpha(L, d)$ of the finite size scaling function for large system sizes. The red dashed line showing the approximate phase boundary is a guide to the eye. Middle: Quasiperiodic angle $\theta = \pi/6.2$ with extended critical phase. The transition point can be estimated to be at $\ln d^{-1} = 1.94$. We use $N = 500$ configurations of the phases $\gamma_{1,2}$ to determine $\alpha(L, d)$ for each data point. Red and blue dashed lines mark the limiting value of α at the critical point (crossing) and in the extended critical phase. Right: The first few iterations of a toy model real-space renormalization group applied to the quasiperiodic network model. The flow of detunings d from the self-dual point is associated with the RG eigenvalue ν^{-1}, the inverse correlation length exponent. For $\theta < \pi/6.4$, there is a region where small, but finite, detunings d are exactly marginal.

is a quantity suitable for a finite size scaling (FSS) study to diagnose criticality [15]. Here division by N_B (the number of boxes) counters the sum over all boxes. Close to criticality (measured by a parameter d) and for large systems, this quantity obeys the scaling form $\alpha(L, d) = \alpha(L(d - d_c)^{-\nu})$, ignoring leading irrelevant corrections [28]. Since we have open boundary conditions, we need to drop the layer of μ_i adjacent to the boundary.

III. PHASE DIAGRAM OF QP CHALKER-CODDINGTON NETWORK

In this section, we investigate the extended critical phase appearing in quasiperiodic quantum Hall transition in Sec. III A and contrast that with the direct transition in Sec. III B. Further we look into the dynamical properties of the network interpreted as a Floquet circuit in Sec. III D.

A. Extended critical phase

We find the phase diagram of the quasiperiodic network model using this scaling theory approach. Remarkably, there is an extended critical phase not present in the random U(1) CC network around the self-dual line. In the left panel of Fig. 2, we show the derivative $\partial_L \alpha(L, d)$ of the finite size scaling function for large system sizes. We identify the different phases as follows: $L \to \infty$ and $\partial_L \alpha(L, d) > 0$ in the insulator, $\partial_L \alpha(L, d) < 0$ in the metal, and at critical points $\partial_L \alpha(L, d) = 0$. At the critical point, the FSS amplitude α is constant and characterizes the fractality of wave functions. In two dimensions, it can be challenging to distinguish bad metals from true asymptotic critical points since the corresponding renormalization group (RG) flows in the uncorrelated case can be as slow as logarithmic in L [29]. In IQH symmetry class A such effects are conventionally not present at strong randomness, and the criticality we observe in the finite size systems here is a genuine feature of the quasirandomness whether or not it persists to $L \to \infty$.

For certain angles, we perform a more detailed finite size scaling analysis with higher resolution in d. For example, for the quasiperiodic angle $\theta = \pi/6.2$ that supports the extended critical phase, we estimate the transition between critical and insulating phases to be at $\ln d^{-1} = 1.94$. The critical phase we find seems to have a constant value of α, which differs from the value of α at the critical end point at $\ln d^{-1} = 1.94$. Our data are shown in the middle panel of Fig. 2.

We support our finding of a critical phase by studying a toy model for real-space RG applied to the quasiperiodic network model [25,30,31]. We compute the flow of detunings d from the self-dual point; the RG eigenvalue ν^{-1} of d is the correlation length exponent. For $\theta < \pi/6.4$, there is a region where small, but finite, detunings d are exactly marginal (stable extended critical phase, black in Fig. 2, right). This qualitatively matches the exact diagonalization result. (Note that the real-space renormalization group is not asymptotically exact for this model, so one does not expect quantitative agreement with numerics.)

B. Direct transition

We now turn to values of θ for which a direct transition between two insulating phases persists in the quasiperiodic case. For the determination of the universal localization length exponent ν, we use the finite size function $\alpha(L, d)$ defined in Eq. (5). In Fig. 3, we show results for two different quasiperiodic potentials with a direct transition. For the determination of the data points, we use linear system sizes $L = 12$, 24, 36, 48, 72, 84, 96, 120, 144, 168, 192, 216, 240, 288, 336, 384, 480, 540, 600 with $N = 500$ configurations of the phases $\gamma_{1,2}$ each. The statistical errors are of the order of the point size.

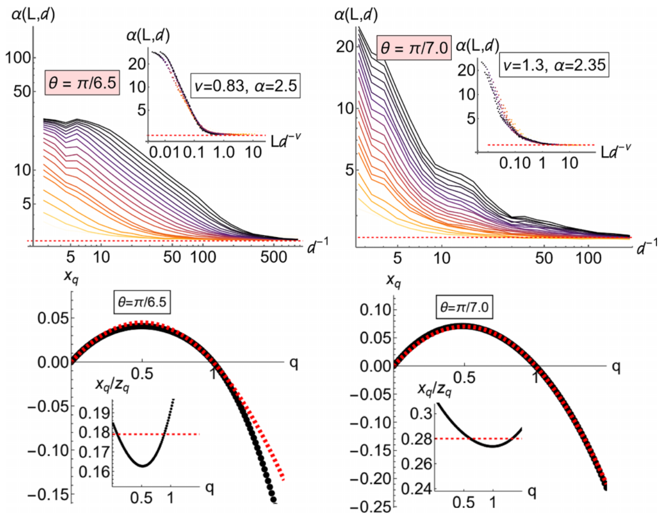

FIG. 3. Localization length exponent. Determination of the universal localization length exponent ν using a finite size function $\alpha(L, d)$ defined in Eq. (5). Different colors represent different system sizes. In the insets finite size collapses are shown. Top left: Quasiperiodic angle $\theta = \pi/6.5$ with fast flow away from the critical point $\nu \approx 0.8 \pm 0.05$. Top right: Quasiperiodic angle $\theta = \pi/7.0$ with slow flow away from the critical point $\nu \approx 1.3 \pm 0.1$. Bottom: Multifractal scaling dimensions x_q in comparison to parabolic form βz_q (dashed red line).

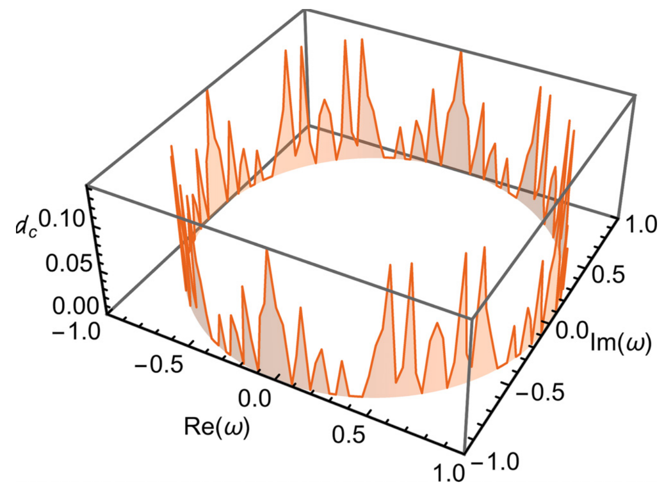

FIG. 4. Quasienergy spectrum. Quasienergy dependence of the transition d_c to the extended critical phase ($\theta = \pi/6.2$). For a direct transition between the topological phases, we put $d_c = 0$. The Re/Imω plane is the complex quasienergy plane; the spectrum of the unitary Chalker-Coddington scattering matrix lies on the unit circle. The d_c axis shows the maximum extent of the critical phase at a given quasienergy ω on the unit circle.

For the fits determining the critical exponent, we take only $L \geqslant 96$ into account. For the quasiperiodic angle $\theta = \pi/6.5$ shown in the top left panel of Fig. 3 we find fast flow away from the critical point with the exponent $\nu \approx 0.8 \pm 0.05$. In the top right panel, we show the angle $\theta = \pi/7.0$ with slow flow away from the critical point $\nu \approx 1.3 \pm 0.1$. Given the long length scales involved in the moiré patterns, we cannot exclude a scenario where these exponents will eventually flow to $\nu = 1$ in the thermodynamic limit. Recall that, by the Harris criterion, $\nu \geqslant 1$ in two dimensions would imply the stability of the two-tone quasiperiodic critical point in the presence of additional weak uncorrelated randomness. With the available system sizes we are unable to definitively address this question, but it remains an interesting one for future work.

C. Nonuniversal multifractal spectra

In the conventional uncorrelated random case, the IQH multifractal spectrum is a universal property of the critical point. The multifractal spectrum is defined by the scaling of the qth participation ratios:

$$\mathcal{P}_q \equiv \frac{1}{N_B}\left\langle \sum_i (\mu_i)^q \right\rangle \sim (b/L)^{2q+x_q}. \tag{6}$$

These anomalous dimensions encode the information about the fractal dimensions $f(\alpha)$ of the sets where the wave function scales as $L^{-\alpha}$; more precisely, (q, x_q) is the Legendre transform of $(\alpha, f(\alpha))$, and the technical mathematical construction is reviewed in Ref. [32]. Typically, the spectrum is approximately parabolic $x_q \approx \beta q(1-q) \equiv \beta z_q$.

In the quasiperiodic case we find, once again, that these spectra behave quite differently for the direct transitions at $\theta = \pi/6.5$ and at $\theta = \pi/7$. For the determination of multifractal spectra, we use $N = 10^4$ configurations of the phases $\gamma_{1,2}$. In the bottom panels of Fig. 3 we show the multifractal spectra x_q for these two cases. The black dots are data points from a fit of the exponent over system sizes $L = 96, 144, 216, 336, 480, 600$. For $\theta = \pi/6.5$, we observe $\beta \approx 0.18$ and approximate parabolicity. The spectrum is not universal because for $\theta = \pi/7.0$, we observe a different curvature $\beta \approx 0.28$. In Appendix A, we analyze different points in the phase diagram that show more irregular behavior of the scaling dimensions x_q.

D. Dynamical properties

Here we study the quasienergy dependence in the network model and the corresponding implications for its dynamical properties in several observables.

1. Quasienergy dependence of phases

If one regards the network model as a Floquet system [27], the eigenstates of the model are labeled by a *quasienergy* ω. The quantum Hall problem nominally corresponds to $\omega = 0$, although there are indirect ways to extract transport properties from ω dependence [33]. An important point to note is that in the uncorrelated random problem the wave function statistics and level repulsion behavior of all ω are the same at the distribution level.

In our quasiperiodic problem, we now consider how the spectrum at general ω evolves as one tunes d (Fig. 4) for an angle $\theta = \pi/6.2$ where an intermediate metallic phase exists at $\omega = 0$. The finite ω spectrum can be probed, for example, in atomic or optical systems that directly realize the network model. Just like the θ dependence, we find that the ω dependence is also highly irregular, with multiple lobes of intermediate extended criticality separated by quasienergies

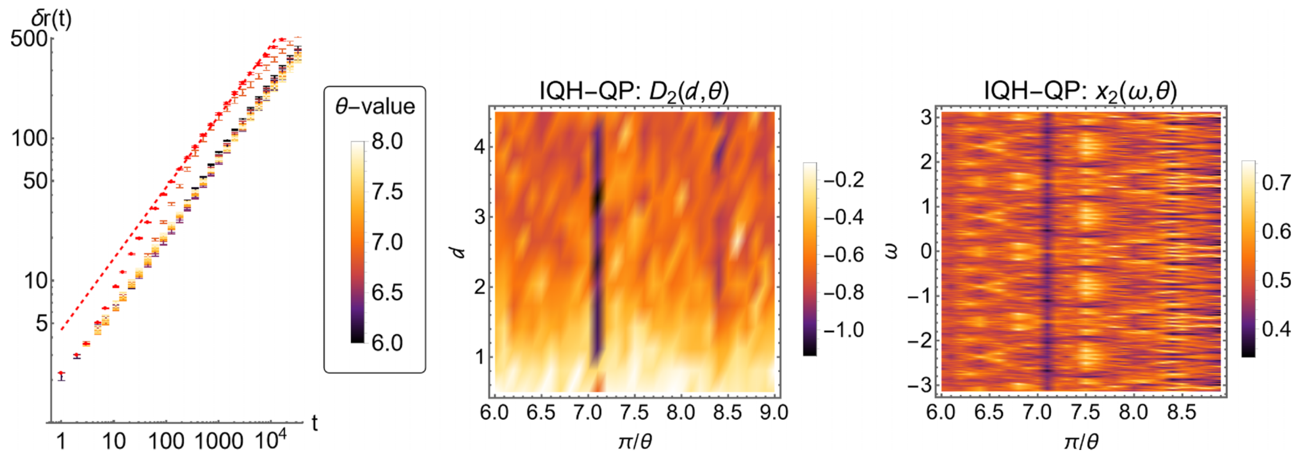

FIG. 5. Dynamical properties of the quasiperiodic U(1) CCN. Comparison of return probability to IPR scaling for a range of $\theta = \pi/6.0$ to $\theta = \pi/9.0$. Left: Spread $\delta r(t)$ as a function of time t for random (red) vs quasiperiodic phases (sunset) at the self-dual point Middle: The extended critical phase for $\theta = \pi/6.0$ leaves a visible imprint. Right: The IPR shows a complex (probably fractal) dependence across the quasienergy spectrum.

for which one has a direct transition. This quasienergy dependence has interesting implications for the dynamics of the network, which is studied in the following sections.

2. Return probability

A well-established observable in the context of dynamics is the return probability:

$$\langle P(t)\rangle = \langle |\langle\psi(t)|\psi(0)\rangle|^2\rangle, \quad \psi(t) = \sum_n \langle\psi_n|\psi(0)\rangle e^{int}|\psi_n\rangle. \tag{7}$$

Results for time evolution simulations are given in the left panel of Fig. 5. We show $D_2(d, \theta)$ as a function of the quasiperiodic angle θ and distance from the critical point d. There is a pronounced dependence on both of these quantities.

3. Wave packet spread

We study the time evolution of an initially localized wave packet $\psi(0)$ in our quasiperiodic system. The complex quasienergy landscape (see Fig. 4) adds features compared to the uncorrelated random case where every level behaves statistically the same.

For an initially fully localized wave packet $\langle\mathbf{r}|\psi(0)\rangle = \delta_{\mathbf{r},\mathbf{r}_0}$ at $\mathbf{r}_0 = 0$ all quasienergies and momenta are involved. The width $\delta\mathbf{r}(t) = \mathbf{r}(t) - \mathbf{r}_0$ usually grows diffusively at criticality:

$$\langle\delta r^2(t)\rangle = \langle\psi(t)|(\mathbf{r} - \mathbf{r}_0)^2|\psi(t)\rangle \sim Dt. \tag{8}$$

In Fig. 5, we show the spread $\delta r(t)$ as a function of time t for the random Chalker-Coddington network (CCN) compared to one with quasiperiodic phases at the self-dual point. Diffusion is present irrespective of the quasiperiodic parameter, and even the numerical value of the diffusion constant is quite insensitive to the angle θ.

4. Inverse participation ratio

We investigate the quasienergy dependence of the second inverse participation ratio (IPR):

$$\langle|\psi_n^2(\mathbf{r})|^2\rangle \sim L^{-x_2(\epsilon_n)}. \tag{9}$$

For the uncorrelated random U(1) CCN the wave functions at all quasienergies obey the same statistical properties (see discussion in Refs. [25,33]), so the multifractal exponent x_2 and the wave packet spread D_2 are trivially related,

$$t^{-D_2} \sim \langle P(t)\rangle \sim \sum_n \int \mathrm{d}\mathbf{r}\ \langle|\psi_n(\mathbf{r})\psi_n(\mathbf{r})|^2\rangle \sim L^{-2x_2}, \tag{10}$$

since each term in the sum scales with the same power. In the quasiperiodic case, there is a complicated dependence of $x_2(\theta, \omega)$ on both the quasiperiodic angle θ and quasienergy ω. We show the results in the right panel of Fig. 5. Nevertheless, there are clear correlations of $x_2(\theta, \omega)$ to $D_2(d \to 0, \theta)$ (compare the upper regions in the middle and right panels of Fig. 5).

IV. CROSSOVER TO RANDOM BEHAVIOR

The plateau transitions we found in the two-tone quasiperiodic model are strikingly different from the random case. We now discuss the crossovers that occur when one modifies the model to make it more like the random one by adding more Fourier components (i.e., more tones) to the spatial modulation in Eq. (1). For simplicity we consider adding one additional incommensurate wavelength.

A. QP Chalker-Coddington network

When the two quasiperiodic modulations have the same strength, we find that the plateau transition is direct, with no intermediate critical phase, and the critical exponent is numerically close to the IQH transition exponent $\nu_{\mathrm{IQH}} \approx 2.4$ [32] (see Fig. 6). At this point a comment is in order: high-precision transfer matrix simulations of very long ($L = 10^9$) strips obtain a different value, $\nu_{\mathrm{IQH}} \approx 2.59$ [34]. The sizes

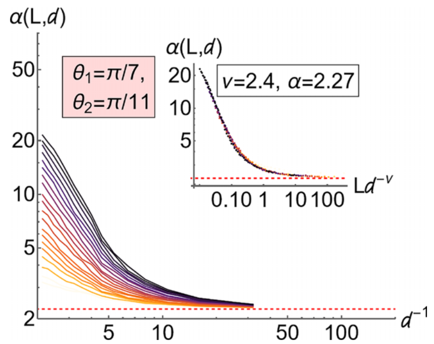

FIG. 6. Crossover to random behavior for multiple tones. The value of ν crosses over the universal value $\nu \approx 2.4$ of the U(1) CCN when two quasiperiodic potentials with $\theta = \pi/7$ and $\theta = \pi/11$ are combined. The plot is analogous to the top panels of Fig. 3.

considered there exceed the typical unit cell size of the QH moiré systems this work was motivated by. In Appendix B, we present further supporting evidence for the conjecture that the presence of multiple tones leads to a crossover to the conventional uncorrelated random critical point. Interestingly, the crossover to the random critical point does not seem to occur when the second modulation is sufficiently weak: rather, the critical properties abruptly jump at some value of this modulation. The corresponding analysis is shown in Fig. 9 in Appendix B.

B. QP Ando model

In order to further support our claim for the crossover to randomness, we demonstrate this effect also occurs in a different model and universality class, the Ando model introduced in Sec. II B.

We determinate the universal localization length exponent ν using the finite size function $\alpha(L, d)$ defined in Eq. (5). Here the distance to the critical point V_c is defined in terms of the strength of the potential $d = (V - V_c)/V_c$. We use linear system sizes $L = 36, 48, 72, 84, 96, 120, 144, 168, 192, 216$ and $N = 5000$ phase configurations. The result is shown in Fig. 7. Different colors represent different system sizes. In the insets finite size collapses are shown. We compare the quasiperiodic case with a single tone $\theta = \pi/8$ to the quasiperiodic case with $\theta = \pi/8$ and a second tone $\theta = \pi/6$ with equal strength and the random uncorrelated potential case. For the one-tone case, the result agrees very well with the findings of Ref. [15]. In the two-tone case, the critical exponent and FSS amplitude approach the ordinary Anderson transition (AT) values exhibited at the random uncorrelated symplectic metal insulator transition, thus supporting our crossover claim also in this symmetry class.

The spin degree of freedom increases the required matrix representation size and makes it computationally challenging to reach the necessary system sizes. We therefore leave a transfer matrix analysis of this model to future work.

V. DISCUSSION

We studied the U(1) Chalker-Coddington model with quasiperiodically modulated link phases. The critical properties of this model are distinct from the uncorrelated random version, which features (topological) insulator phases separated by critical points that can be reached only by fine-tuning the energy or magnetic field. In the quasiperiodic case, the nature of the phase diagram is sensitive to the angle θ between the underlying lattice and the superimposed quasiperiodic modulation. For a range of θ we find a critical phase between the two insulators. In the quantum Hall context, this means that quantized Hall plateaus are separated by a regime with nonvanishing longitudinal conductivity and a nonquantized Hall response. For other values of θ we find a direct plateau transition; the associated critical exponent is clearly incompatible with the random case. The critical exponent ν that we find appears nonuniversal and θ dependent, ranging from $\nu = 0.80(5)$ to $\nu = 1.3(1)$. However, the flow to the insulating phase is slow, and we cannot be sure these exponents are really distinct; in any case they are very far from the random value $\nu \approx 2.4$. Moreover, the multifractal spectra in the quasiperiodic case also seem to be nonuniversal. Determining these exponents more accurately and identifying whether they are

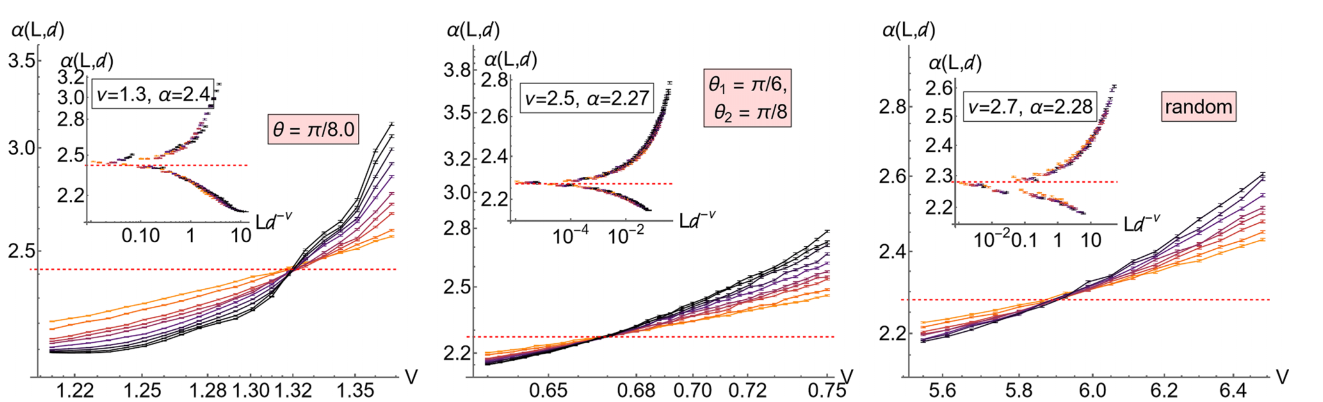

FIG. 7. Finite size scaling analysis in the Ando model. Determination of the universal localization length exponent ν using a finite size function $\alpha(L, d)$ defined in Eq. (5) in the Ando model where w is the potential strength. Different colors represent different system sizes. In the insets finite size collapses are shown. Left: Quasiperiodic with a single $\theta = \pi/8$. The result agrees very well with the findings of Ref. [15]. Middle: Quasiperiodic with $\theta = \pi/8$ and a second tone $\theta = \pi/6$ with equal strength. The critical exponent and FSS amplitude approach the ordinary AT values. Right: Random uncorrelated potential; the model is the conventional Ando model [32] in this limit.

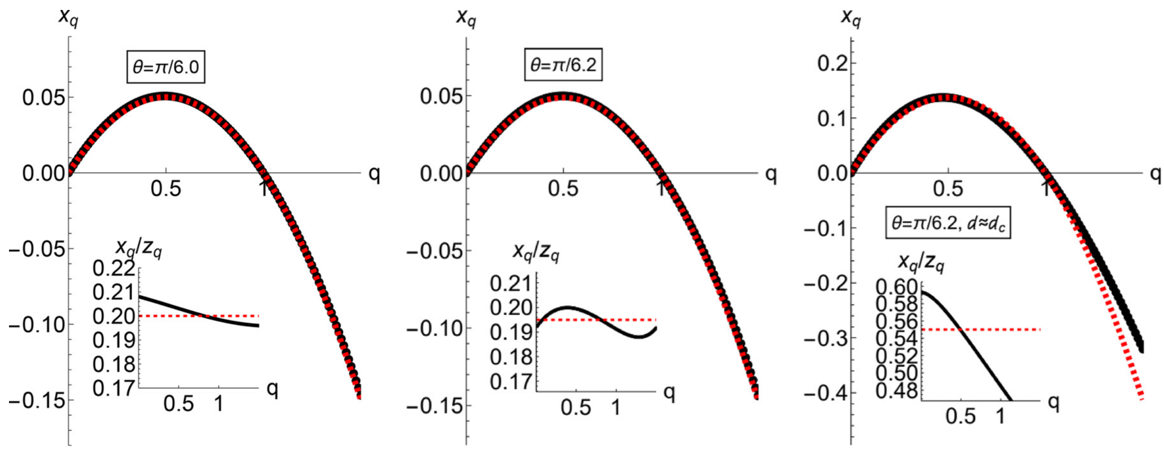

FIG. 8. Multifractal spectra x_q for various quasiperiodic angles θ. Black dots are data points from a fit of the exponent over system sizes $L = 96$–600. Left: Close to the boundary of the extended critical phase for $\theta = \pi/6.0$ Middle: Deep in the metallic phase $\theta = \pi/6.2$ and $d = 0.0$. The result is very similar to the data shown in the right panel. Right: Novel critical point for $\theta = \pi/6.2$ and $d = 0.11 \approx d_c$. There is strong multifractality, and the multifractal spectrum is still approximately parabolic.

stable with respect to the Harris bound $\nu = 1$ are interesting questions for future work. The irregular dependence of the phase diagram and exponents on the quasiperiodic angle θ and the quasienergy ω—as well as the sensitivity of the exponents to adding additional modulations—suggests that these quantities are sensitive to high-order scattering processes that depend on the precise kinematics of the quasiperiodic potential. It remains an open challenge to develop an analytic framework for understanding this dependence. It would also be interesting to develop a scaling theory of transport in the critical phase and to look for similar critical phases in quasiperiodic systems in other Altland-Zirnbauer symmetry classes [23].

ACKNOWLEDGMENTS

We acknowledge discussions with I. Gruzberg. J.F.K. is supported by the Army Research Office under the MURI program, Grant No. W911NF-22-2-0103. We acknowledge support from NSF Grants No. DMR-2103938 (S.G.) and No. DMR-2104141 (R.V.) and the Alfred P. Sloan Foundation through Sloan Research Fellowships (R.V.).

APPENDIX A: MULTIFRACTAL SPECTRA IN THE METALLIC PHASE AND ON THE CRITICAL LINE

Here we extend the analysis of the multifractal spectrum presented in Fig. 3. The multifractal spectrum is defined by the scaling of the qth participation ratio:

$$\mathcal{P}_q \equiv N_B^{-1}\left\langle \sum_i (\mu_i)^q \right\rangle \sim (b/L)^{2+x_q}. \tag{A1}$$

The anomalous dimensions x_q encode the information about the fractal dimensions $f(\alpha)$ of the sets where the wave function scales as $L^{-\alpha}$; more precisely, (q, x_q) is related to $(\alpha, f(\alpha))$ by a Legendre transform [32]. Typically, the spectrum is approximately parabolic, $x_q \approx \beta q(1-q) \equiv \beta z_q$. The Weyl symmetry relation $x_q = x_{1-q}$ constrains random class A Anderson transition multifractal spectra [32].

In Fig. 8, we show multifractal spectra x_q for various quasiperiodic angles θ. Black dots are data points from a fit of the exponent over system sizes $L = 96$–600. We show data for a point in the phase diagram close to the boundary of the extended critical phase for $\theta = \pi/6.0$ and deep in the metallic phase for $\theta = \pi/6.2$ and $\ln d^{-1} = 0.0$. These behave strikingly similarly. Finally, we show data for the critical point for $\theta = \pi/6.2$ and $d = 0.11 \approx d_c$. There is strong multifractality, and the multifractal spectrum is still approximately parabolic. In particular the transition at $\theta = \pi/6.2$ displays strong violations of the symmetry relation $x_q = x_{1-q}$ that holds exactly in the uncorrelated random case.

APPENDIX B: CROSSOVER TO RANDOMNESS FOR MANY TONES: QP CC TRANSFER MATRIX

In this Appendix, we demonstrate the crossover from the quasiperiodic to the random fixed point as tones are added in the quasiperiodic potential. We do so using transfer matrix studies of the U(1) CCN in class A.

We provide additional numerical data to support the conjecture on the crossover between randomness and quasiperiodic fixed points (see Fig. 6). We perform a transfer matrix analysis of a quasi-1D (Q1D) $L \times W$ strip of the system with $L \gg W$. The observable we study is the second Lyapunov exponent ξ_W. In the limit $W \to \infty$, the ratio ξ_W/W is an observable suitable for finite size scaling near criticality.

We can write the network model scattering matrix (see Fig. 1; colors are chosen to match link colors there) as

$$\begin{aligned} &\begin{pmatrix} c^{-1}e^{i\epsilon}e^{-i\phi_{t+1,u}} & sc^{-1}e^{-i\phi_{t+1,u}}e^{i\phi_{t,u+1}} \\ sc^{-1} & (c+s^2c^{-1})e^{-i\epsilon}e^{i\phi_{t,u+1}} \end{pmatrix}\begin{pmatrix} \ell_{t,u} \\ \ell_{t,u+1} \end{pmatrix} \\ &\quad = \begin{pmatrix} \ell_{t+1,u} \\ \ell_{t+1,u+1} \end{pmatrix}, \\ &\begin{pmatrix} s^{-1}e^{i\epsilon}e^{-i\phi_{t+2,u}} & -s^{-1}ce^{-i\phi_{t+2,u}}e^{i\phi_{t+1,u-1}} \\ -s^{-1}c & (s+s^{-1}c^2)e^{-i\epsilon}e^{i\phi_{t+1,u-1}} \end{pmatrix}\begin{pmatrix} \ell_{t+1,u} \\ \ell_{t+1,u-1} \end{pmatrix} \\ &\quad = \begin{pmatrix} \ell_{t+2,u} \\ \ell_{t+2,u-1} \end{pmatrix} \end{aligned} \tag{B1}$$

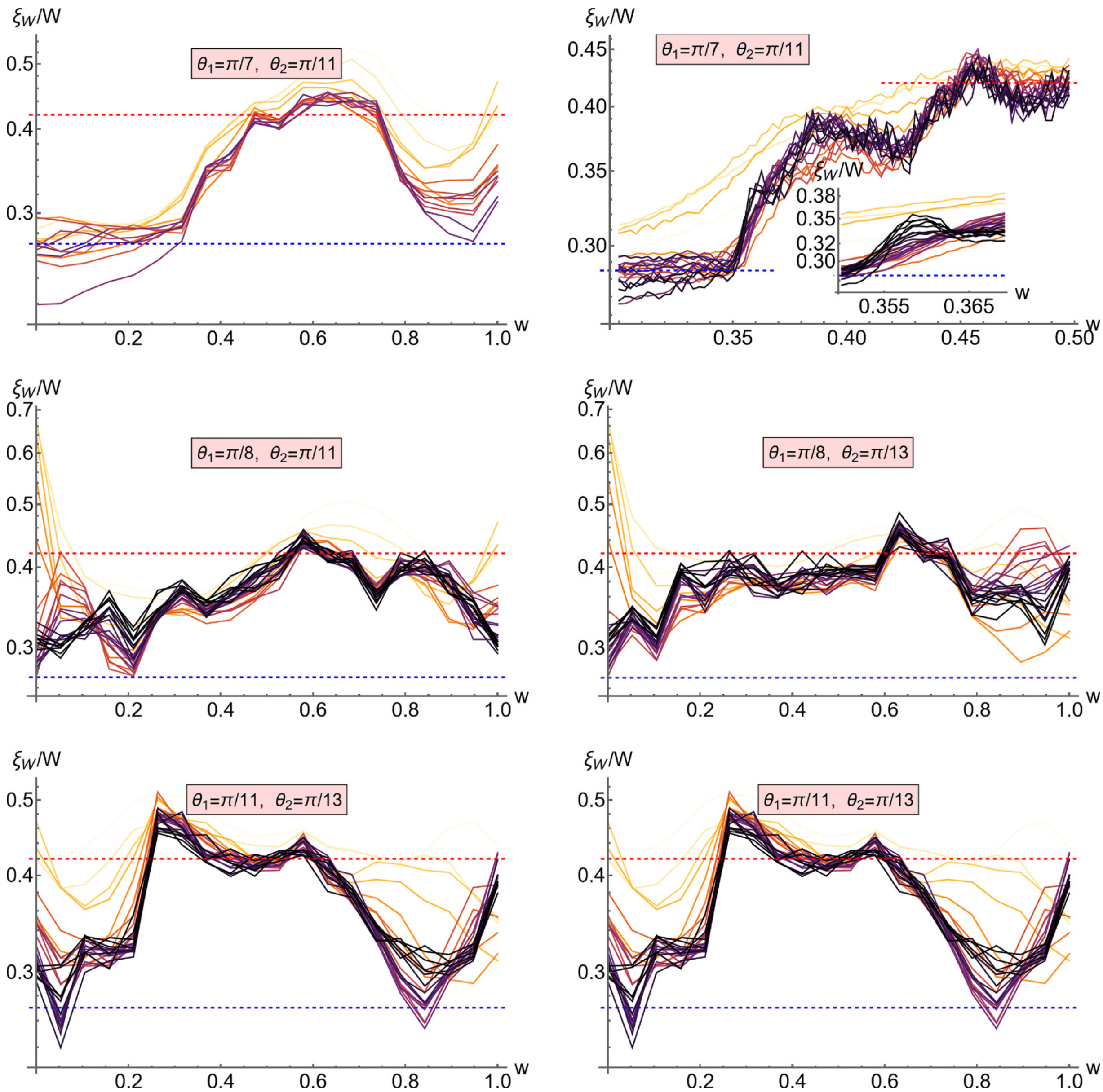

FIG. 9. Crossover between randomness and quasiperiodic fixed points. The observable we study is the second Lyapunov exponent ξ_W of a quasi-1D $L \times W$ strip of the system. We interpolate between different quasiperiodic link modulations with a parameter w. At $w = 0$ (or 1) only one (or the other) tone is present, and at $w = 0.5$ they are evenly mixed. Dashed red and blue lines are guides to the eye for QP and a random value of ξ_W.

in order to find the transfer matrix of the system relating the link amplitudes $\ell_{t+1,u}$ of slice t to those of slice $t+1$. Using standard methods [25], we can find all Lyapunov exponents of a Q1D strip.

We interpolate between quasiperiodic link modulations with two different θ using the parameter $w \in [0, 1]$:

$$\phi(r) = w\phi_1(r) + (1-w)\phi_2(r),$$

$$\phi_k(r) = 2\pi \sum_{i=1,2} \cos\left(\sum_j A_{ij}^{(k)} r_j + \gamma_i\right),$$

$$A_{11}^{(k)} = A_{22}^{(k)} = \varphi\cos\theta_k, A_{12}^{(k)} = -A_{21}^{(k)} = \varphi\sin\theta_k. \tag{B2}$$

At $w = 0$ (or $w = 1$) only one tone is present, and at $w = 0.5$ the two tones are perfectly mixed. In this way, we can see the random/QP crossover for different QP parameters. For the numerical calculations, we choose $W = 12$, 16, 24, 32, 48, 64, 80, 96, 112, 128, 144, 160, 176, 192, 208, 224, 240, 256, 272, 288, 304, 320, 336, 352, 368, 384 and $L = 10^5$. In Fig. 9, we show additional supporting data on the crossover between randomness and quasiperiodic fixed points. It does not seem to occur when the second modulation is sufficiently weak; instead, ξ_W/W shows a discontinuous jump at a finite value, $1 > w_c > 0$, of the interpolation. This effect seems to be generic, as it appears for various pairs of θ_1, θ_2.

[1] S. Girvin and R. Prange, The quantum Hall effect, in *Topological Aspects of Low Dimensional Systems*, edited by A. Comtet, T. Jolicoeur, S. Ouvry, F. David (Springer-Verlag, Berlin and Les Editions de Physique, Les Ulis, 2000).
[2] H. P. Wei, D. C. Tsui, M. A. Paalanen, and A. M. M. Pruisken, Experiments on delocalization and university in the integral quantum Hall effect, Phys. Rev. Lett. **61**, 1294 (1988).
[3] A. M. M. Pruisken, Universal singularities in the integral quantum Hall effect, Phys. Rev. Lett. **61**, 1297 (1988).
[4] A. Pruisken, On localization in the theory of the quantized Hall effect: A two-dimensional realization of the θ-vacuum, Nucl. Phys. B **235**, 277 (1984).
[5] M. R. Zirnbauer, The integer quantum Hall plateau transition is a current algebra after all, Nucl. Phys. B **941**, 458 (2019).
[6] J. F. Karcher, N. Charles, I. A. Gruzberg, and A. D. Mirlin, Generalized multifractality at spin quantum Hall transition, Ann. Phys. (NY) **435**, 168584 (2021).
[7] J. F. Karcher, I. A. Gruzberg, and A. D. Mirlin, Generalized multifractality at the spin quantum Hall transition: Percolation mapping and pure-scaling observables, Phys. Rev. B **105**, 184205 (2022).
[8] O. Zilberberg, S. Huang, J. Guglielmon, M. Wang, K. P. Chen, Y. E. Kraus, and M. C. Rechtsman, Photonic topological boundary pumping as a probe of 4D quantum Hall physics, Nature (London) **553**, 59 (2018).
[9] F. He, Y. Zhou, Z. Ye, S.-H. Cho, J. Jeong, X. Meng, and Y. Wang, Moiré patterns in 2D materials: A review, ACS Nano **15**, 5944 (2021).
[10] T. Shimasaki, M. Prichard, H. Esat Kondakci, J. E. Pagett, Y. Bai, P. Dotti, A. Cao, A. R. Dardia, T.-C. Lu, T. Grover, and D. M. Weld, Anomalous localization in a kicked quasicrystal, Nat. Phys. (2024), doi: 10.1038/s41567-023-02329-4.
[11] D. Morison, N. B. Murphy, E. Cherkaev, and K. M. Golden, Order to disorder in quasiperiodic composites, Commun. Phys. **5**, 148 (2022).
[12] S. Vaidya, C. Jörg, K. Linn, M. Goh, and M. C. Rechtsman, Reentrant delocalization transition in one-dimensional photonic quasicrystals, Phys. Rev. Res. **5**, 033170 (2023).
[13] S. Aubry and G. André, Analyticity breaking and Anderson localization in incommensurate lattices, Ann. Israel Phys. Soc. **3**, 133 (1980).
[14] B. Kramer and A. MacKinnon, Localization: Theory and experiment, Rep. Prog. Phys. **56**, 1469 (1993).
[15] T. Devakul and D. A. Huse, Anderson localization transitions with and without random potentials, Phys. Rev. B **96**, 214201 (2017).
[16] S. Gopalakrishnan, Self-dual quasiperiodic systems with power-law hopping, Phys. Rev. B **96**, 054202 (2017).
[17] J. H. Pixley, J. H. Wilson, D. A. Huse, and S. Gopalakrishnan, Weyl semimetal to metal phase transitions driven by quasiperiodic potentials, Phys. Rev. Lett. **120**, 207604 (2018).
[18] Y. Fu, E. J. König, J. H. Wilson, Y.-Z. Chou, and J. H. Pixley, Magic-angle semimetals, npj Quantum Mater. **5**, 71 (2020).
[19] M. Rossignolo and L. Dell'Anna, Localization transitions and mobility edges in coupled Aubry-André chains, Phys. Rev. B **99**, 054211 (2019).
[20] Y.-Z. Chou, Y. Fu, J. H. Wilson, E. J. König, and J. H. Pixley, Magic-angle semimetals with chiral symmetry, Phys. Rev. B **101**, 235121 (2020).
[21] A. Szabó and U. Schneider, Mixed spectra and partially extended states in a two-dimensional quasiperiodic model, Phys. Rev. B **101**, 014205 (2020).
[22] A. Štrkalj, E. V. H. Doggen, and C. Castelnovo, Coexistence of localization and transport in many-body two-dimensional Aubry-André models, Phys. Rev. B **106**, 184209 (2022).
[23] A. Altland and M. R. Zirnbauer, Nonstandard symmetry classes in mesoscopic normal-superconducting hybrid structures, Phys. Rev. B **55**, 1142 (1997).
[24] J. T. Chalker and P. D. Coddington, Percolation, quantum tunnelling and the integer Hall effect, J. Phys. C **21**, 2665 (1988).
[25] B. Kramer, T. Ohtsuki, and S. Kettemann, Random network models and quantum phase transitions in two dimensions, Phys. Rep. **417**, 211 (2005).
[26] N. Goldman, G. Juzeliūnas, P. Öhberg, and I. B. Spielman, Light-induced gauge fields for ultracold atoms, Rep. Prog. Phys. **77**, 126401 (2014).
[27] A. C. Potter, J. T. Chalker, and V. Gurarie, Quantum Hall network models as Floquet topological insulators, Phys. Rev. Lett. **125**, 086601 (2020).
[28] K. Slevin and T. Ohtsuki, Corrections to scaling at the Anderson transition, Phys. Rev. Lett. **82**, 382 (1999).
[29] J. F. Karcher, I. A. Gruzberg, and A. D. Mirlin, Generalized multifractality at metal-insulator transitions and in metallic phases of two-dimensional disordered systems, Phys. Rev. B **106**, 104202 (2022).
[30] A. G. Galstyan and M. E. Raikh, Localization and conductance fluctuations in the integer quantum Hall effect: Real-space renormalization-group approach, Phys. Rev. B **56**, 1422 (1997).
[31] D. P. Arovas, M. Janssen, and B. Shapiro, Real-space renormalization of the Chalker-Coddington model, Phys. Rev. B **56**, 4751 (1997).
[32] F. Evers and A. D. Mirlin, Anderson transitions, Rev. Mod. Phys. **80**, 1355 (2008).
[33] R. Klesse and M. Metzler, Spectral compressibility at the metal-insulator transition of the quantum Hall effect, Phys. Rev. Lett. **79**, 721 (1997).
[34] K. Slevin and T. Ohtsuki, Critical exponent for the quantum Hall transition, Phys. Rev. B **80**, 041304(R) (2009).